Aluminium alloy processed by square-column composite structure and its anti-icing characteristics

Yanling Wan ✉, *Meng Zhang, Bin Dong, Huadong Yu*

National and Local Joint Engineering Laboratory for Precision Manufacturing and Measurement Techniques, Changchun University of Science and Technology, Changchun 130012, People's Republic of China
✉ *E-mail: wanyl@cust.edu.cn*

Published in Micro & Nano Letters; Received on 22nd March 2019; Revised on 29th January 2020; Accepted on 16th March 2020

To prepare surfaces with stable anti-icing properties, square-column micro/nanocomposite structures were fabricated using wire-cut electrical discharge machining. Smooth and hydrophobic/superhydrophobic surfaces were tested for wettability and were subjected to mechanistic analysis. Droplets were found to produce an 'air cushion effect' upon contact with the microstructure, which reduced the contact area between the droplets and the aluminium substrate and increased the contact angle of the droplets on the surface. The icing experiment quantitatively evaluated the anti-icing performance of the surfaces by observing the cooling time and out-of-phase icing time of water droplets. It was found that the anti-icing effect is influenced by the wettability of the material and that the superhydrophobic surface has excellent anti-icing properties. Combined with the one-dimensional heat transfer theory for analysing the mechanism of icing, the results show that the 'air cushion' reduces the heat transfer between the solid and liquid and increases the thermodynamic barrier to ice core formation. The stability of the sample surface was tested by icing-melting experiments and friction experiments, and the test piece exhibited stable wettability and anti-icing performance.

1. Introduction: Icing is a common natural phenomenon that can increase safety risks and cause economic losses. For example, the safety of aircraft is affected by the freezing of critical components [1]; icing can damage rolling stock and cause traffic accidents [2]; and if communication and electricity transmission lines become iced, the ice needs to be removed to avoid affecting the efficiency of transmission [3, 4]. Methods such as heating, chemical and mechanical approaches [5, 6] are used as common deicing methods. Although these methods can effectively remove the ice on a machine, they have the disadvantages of having low efficiency, wasting resources and even causing environmental pollution. Therefore, the development of surfaces with delayed icing has become a new way to solve the problems of icing.

A surface with a water droplet contact angle >150° and a sliding angle <10° is called a superhydrophobic surface. In recent years, with the development of micro/nanotechnology and bionics, superhydrophobic surfaces with excellent functions such as self-cleaning [7, 8] drag reduction [9], oil–water separation [10] and anti-corrosion [11] have attracted extensive attention.

In the field of anti-icing, many studies have reported that superhydrophobic surfaces may perform better than smooth surfaces [12, 13] because the initial nucleation of droplet icing was delayed by surfaces with a large contact angle [14]. Therefore, researchers have attempted to prepare superhydrophobic surfaces to obtain surfaces with delayed or anti-icing properties [15–17]. Studies have shown that the superhydrophobic properties of the lotus leaf are derived from the micro/nanostructures and waxy crystals on its surfaces [18]. Thus, processing composite structures has become one of the methods for obtaining a superhydrophobic surface. For example, Guo *et al.* [19] processed ratchet-shaped micro/nanocomposite structures on a stainless steel surface by machining and ZnO nanohair planting. The freezing time at −10°C can be delayed to 7220 s. Liu *et al.* [20] obtained a superhydrophobic composite surface by pulsed fibre laser processing and anodising, and the surface showed very good anti-icing performance.

In addition, researchers have successfully prepared composite microstructures by chemical vapour deposition [21], electrochemical and electroless chemical deposition [22] and crystal preferential etching [23] to obtain a superhydrophobic surface and assessed its anti-icing performance.

Although many studies have shown that superhydrophobic surfaces have anti-icing properties, the influence of superhydrophobicity on their anti-icing properties is still inconclusive. There are also reports that superhydrophobic does not necessarily correspond to anti-icing [24]. In addition, the anti-icing ability of superhydrophobic surfaces with the same wettability and different structures is different. The reasons for these results need to be further explored. Therefore, based on the composite structures of the lotus leaf and the characteristics of wire-cut electrical discharge machining (WEDM), square-column composite structures are processed on the surface of aluminium alloy. The anti-icing performance of samples with different wettability was quantitatively evaluated by comparison with the anti-icing performance of smooth surfaces and hydrophobic/superhydrophobic surfaces. The mechanism and stability of the surfaces with delayed icing, which are of great significance for exploring the development of new deicing technology, were also analysed and evaluated.

2. Sample preparation

2.1. Microstructure design: Based on the processing characteristics of WEDM and the micro/nanocomposite structure of the lotus leaf surface, square-column composite structures were designed and are shown in Fig. 1. The top edge length, the column spacing, and the column height of the square-column structures were defined as a, b, and h, respectively.

The Cassie model is a wetting model. When the contact of a droplet with a rough surface corresponds to the Cassie model, trapped air is present beneath the droplet; thus, the droplet does not penetrate the interior of the microstructure, and the solid–liquid interface converts into a solid–gas–liquid interface. To prepare a superhydrophobic surface, the behaviour of droplets on the surface must follow the Cassie model. Therefore, according to the Cassie law [25]

$$\cos\theta_c = -1 + f_s(\cos_e + 1) \tag{1}$$

The area fraction (f_s) of the solid–liquid interface on the surface of the square-column microstructures was

$$f_s = \frac{(a+2h')^2}{(a+b)^2} \tag{2}$$

doi: 10.1049/mnl.2019.0171

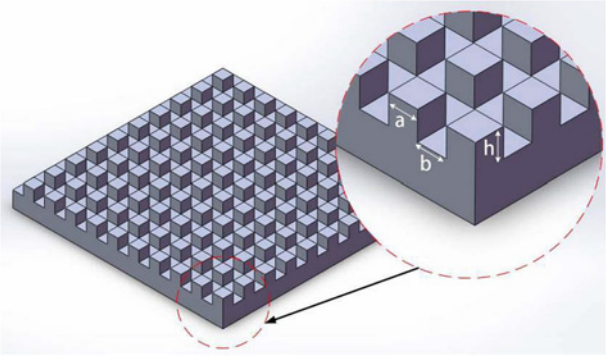

Fig. 1 *Square-column composite structures*

Table 1 Geometric parameters of square-column composite structures

Sample number	a, μm	b, μm	h, μm
no.1 (hydrophobic)	300	300	600
no.2 (superhydrophobic)	300	750	600

where h is the depth at which the droplets were penetrated in the microstructure. Substituting formula (2) into formula (1) yields

$$\cos\theta_c = -1 + \frac{1 + (2h'/a)}{(1 + (b/a))^2}(\cos\theta_e + 1) \quad (3)$$

It is known that the contact angle θ_e of a smooth aluminium alloy surface is 56°. Assume that the droplet was not immersed in the microstructure at all ($h' = 0$). When designing a superhydrophobic surface, assume that the theoretical contact angle of the droplet with the surface is 150°, $\beta_1 = b/a \approx 2.41$; when designing a hydrophobic surface, assume that the theoretical contact angle of the droplet with the surface is 125°, $\beta_2 = b/a \approx 0.9$. For the convenience of calculation, β_1 was taken as 2.5, and β_2 was taken as 1. As shown in (3), the contact angle was not affected by the column height. In combination with the processing conditions of WEDM, the height was taken to be 600 μm. The design dimensions can be seen in Table 1.

2.2. Microstructure preparation: The test material was aluminium alloy 6061 with a sample size of 15 mm × 15 mm × 5 mm. Test reagents include acetone, absolute ethanol, deionised water etc. The aluminium alloy was polished using 400#-2000# sandpaper, and then the surface of the aluminium alloy was machined using a wire electric discharge machine. The machining process is shown in Fig. 2. The machining parameters were as follows: the pulse power supply was 50–70 V, the pulse interval was 84 μs, the pulse width was 12 μs, and the peak current was 1.5 A. The processed workpieces were ultrasonically cleaned in acetone, absolute ethanol and deionised water in turn and naturally dried.

2.3. Characterisation and analysis: The surface morphology of the workpiece was observed using a scanning electron microscope (SEM), and their wettability was detected using a video optical contact angle meter. Deionised water (4 μl) was used to test the wettability of the workpiece. The wettability test was conducted 10 times, and the average value was taken as a result.

2.4. Icing performance: The anti-icing performance of the samples was tested using a homemade icing performance test rig, which consisted mainly of a semiconductor refrigeration module and an image acquisition system (Fig. 3). The initial temperature and initial relative humidity in the anti-icing performance test were

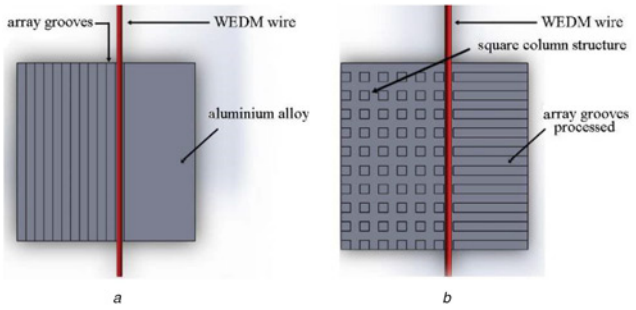

Fig. 2 *Square-column composite structure processing schematic*
a Machined into array grooves on the surface of the polished aluminium alloy
b Rotate the workpiece 90° and perform second machining on the array grooves

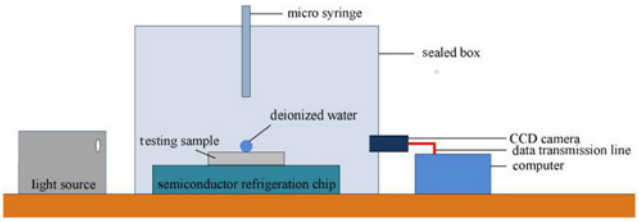

Fig. 3 *Anti-icing performance test bench*

20 ± 3°C and 40%, respectively. When performing the icing performance test, the samples were placed on the refrigeration device, and water droplets of 4 μl were injected onto the surface of the sample. Then, the temperature of the refrigeration device was adjusted to the predetermined temperature, and the droplet freezing process was observed and recorded.

2.5. Stability test: The stability of the superhydrophobic/hydrophobic surface in practical applications was tested by icing-melting experiments and friction experiments. The icing-melting experimental procedure was as follows: a beaker (beaker capacity of 100 ml) was taken, and the superhydrophobic sample was placed into the beaker. Next, 50 ml of deionised water was poured into the beaker, and the beaker was placed in a refrigerator at − 10°C until it was completely frozen. Then, the frozen sample was placed at room temperature, and after the ice was completely melted, the test piece was ultrasonically cleaned in acetone, absolute ethanol and deionised water in turn and naturally dried. After every four icing-melting tests, the contact angle of the test piece and the droplet icing time were measured (surface temperature was −10°C). The friction experimental procedure was as follows: 2000 CW sandpaper was taken, and the workpiece was placed horizontally on the sandpaper; a 20 g weight was placed on the surface of the sample, and the sample was pulled on the surface of the sandpaper with a rubbing distance of 100 mm to reciprocate.

3. Results and analysis

3.1. Surface morphology and wetting properties: The dimensions of the microstructure of the hydrophobic workpiece and superhydrophobic workpiece were measured, and the results are shown in Fig. 4. The top edge length, column height, and column spacing of the hydrophobic surface were 301 ± 9.38, 596 ± 8.89 and 300.7 ± 4.32 μm, respectively; the top edge length, column height, and column spacing of the superhydrophobic surface were 298 ± 6.38, 602 ± 10.89 and 750 ± 6.62 μm, respectively. By comparing the actual dimensions with the design dimensions, it can be seen that the prepared workpieces meet our expectations.

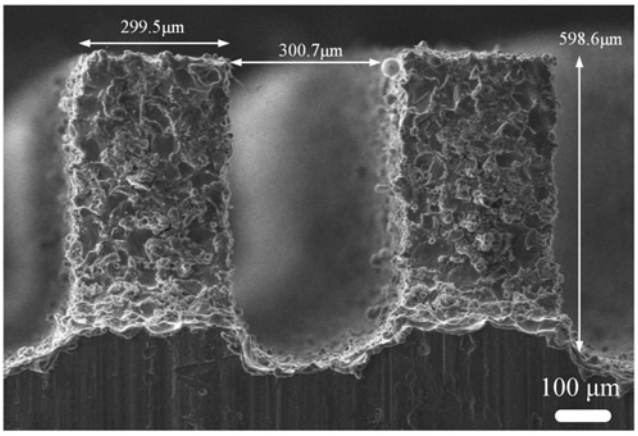

a

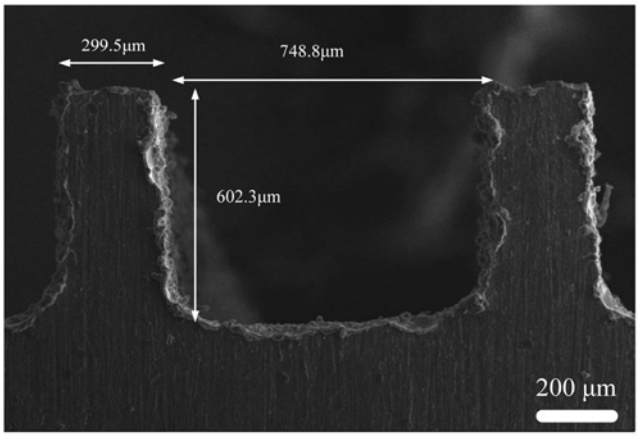

b

Fig. 4 *Dimensions of the square-column structures*
a Hydrophobic sample
b Superhydrophobic sample

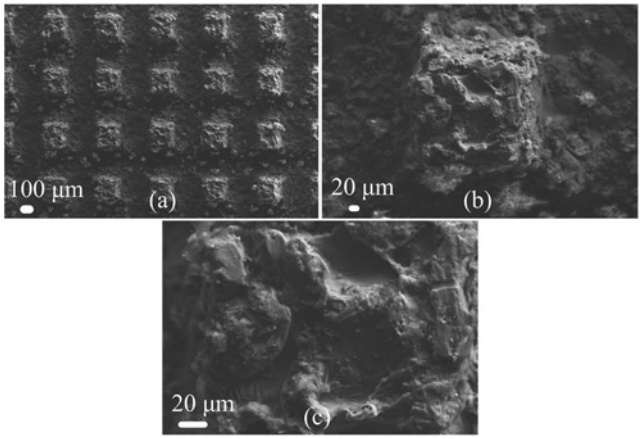

Fig. 5 *SEM images of the microstructure of the superhydrophobic sample*
a Scanned image at low magnification
b Scanned image at medium magnification
c Scanned image at high magnification

SEM images of the square-column composite structures are shown in Fig. 5. Fig. 5*a* shows that the square-column structures constructed on the surface of the aluminium alloy were arranged neatly. Fig. 5*b* shows that there were many convex pit-shaped microscale structures distributed on the surface of the microstructures. When the local structure is further magnified, sub-micron or even nanoscale structures can be found at the top of convex pit-shaped microscale structures (as shown in Fig. 5*c*).

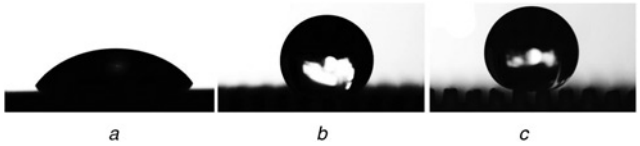

Fig. 6 *Water droplet contact angle images on the specimen surface*
a Smooth specimen surface
b Hydrophobic specimen surface
c Superhydrophobic specimen surface

Therefore, convex pit-shaped microscale structures were formed on the surface of the microstructure, which made the topography of the sample surface more rough and complex by producing an 'air cushion' effect. In addition, due to the instantaneous high temperature generated by the electric field, the working fluid was gasified during processing. The gaseous working fluid condensed and adhered to the surface of the material, increasing the carbon and oxygen content. As a result, the composition of the aluminium alloy surface changed [26]. The micro/nanocomposite structure and the change in the material composition were responsible for the increase in the hydrophobicity of the aluminium alloy.

After measuring the wettability of the test piece, it was found that the droplet exhibited a crown on a smooth surface with a contact angle of 55.35° (Fig. 6*a*); it was also found that the droplets exhibited a spherical shape on the hydrophobic and superhydrophobic surfaces with contact angles of $140.64 \pm 2.68°$ (Fig. 6*b*) and $157.71 \pm 3.42°$, respectively (Fig. 6*c*). One-step preparation of hydrophobic and superhydrophobic aluminium alloy surface is achieved by processing the square-column composite structures onto the aluminium surface.

3.2. Anti-icing experimental results and mechanistic analysis: Droplet icing includes two stages: homogeneous cooling and out-of-phase icing. These stages are represented by the homogeneous cooling time (t_c) and the out-of-phase freezing time (t_f), respectively. The boundary between homogeneous cooling and out-of-phase icing was distinguished by the contact state of the droplets on the surface of the material: in the homogeneous cooling stage, the shape of the droplets changed continuously, while in the stage of out-of-phase icing, the contact state of the droplet on the surface did not change. The surface of the frozen droplet becoming frosted represented the end of the out-of-phase icing stage. Fig. 7 depicts the process of the icing of droplets on the superhydrophobic surface, and the homogeneous cooling stage and out-of-phase icing stage are noted in the figure. The anti-icing performance of the surface of the test piece was evaluated by comparing t_c and t_f. The test results are shown in Fig. 8.

As shown in Fig. 8, both the superhydrophobic surface and the hydrophobic surface exhibited superior anti-icing effects compared to that of the smooth surface. The anti-icing performance of the superhydrophobic surface, hydrophobic surface and smooth surface decreased in turn. When the surface temperature was −5°C, the homogeneous cooling time and out-of-phase icing time of the hydrophobic surface and superhydrophobic surface were larger than those of the smooth surface; as the surface temperature

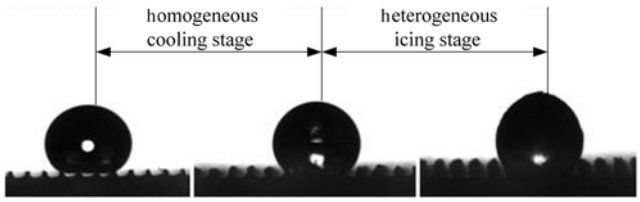

Fig. 7 *Ice formation process on the superhydrophobic surface*

doi: 10.1049/mnl.2019.0171

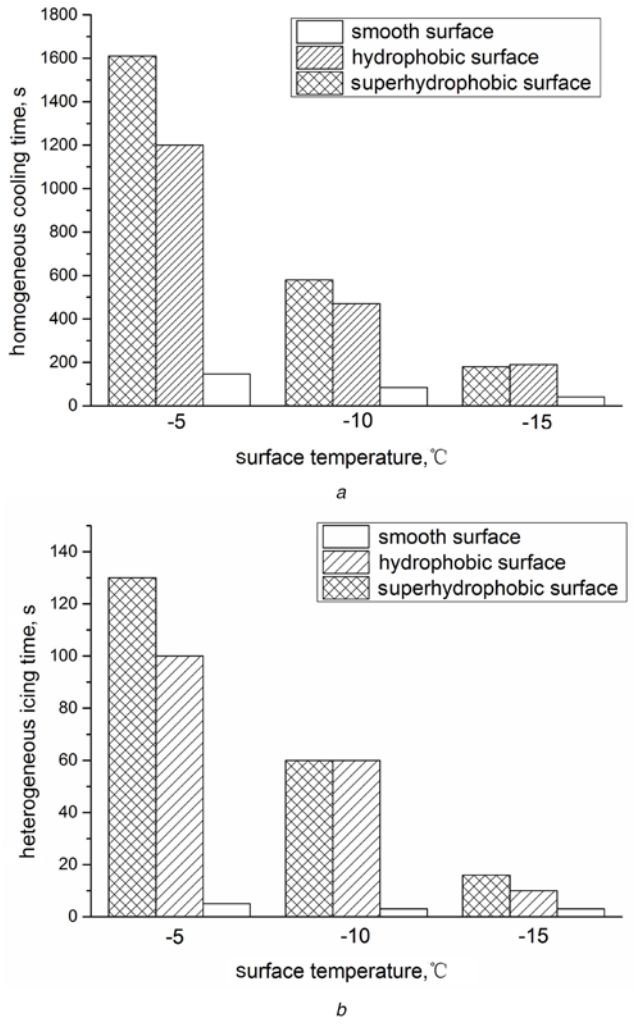

Fig. 8 *Time histogram of the homogeneous cooling stage and out-of-phase icing stage*
a Homogeneous cooling time
b Out-of-phase icing time

continuously decreased, the homogeneous cooling time and out-of-phase icing time of the hydrophobic/superhydrophobic surfaces were greatly reduced. However, compared with the smooth surface, the hydrophobic/superhydrophobic surface still greatly prolonged the duration of the homogeneous cooling stage and the out-of-phase icing stage.

As the temperature continued to decrease, the homogeneous cooling time and out-of-phase icing time of the hydrophobic surface and superhydrophobic surface gradually decreased. When the surface temperature dropped to −15°C, the superhydrophobic surface and the hydrophobic surface showed similar anti-icing effects, which can be explained by the fact that the homogeneous cooling time and the out-of-phase icing time were very similar. It can be seen from the icing time that the hydrophobic surface and the superhydrophobic surface had excellent anti-icing properties but the anti-icing performance was weakened with decreasing temperature.

When water freezes at 0°C, according to the one-dimensional heat transfer theory, the relationship between the time t of delay in the freezing of water droplets and the initial temperature T_0 of cooling was as follows [27, 28]:

$$VT_0 = tK\mathrm{S} \tag{4}$$

where V is the volume of the droplet, K is a constant associated with the surface temperature and the specific heat of the water, and S is the actual contact area of the water droplet with the surface. Therefore, the time at which the droplet delays freezing was proportional to the value of V/S

$$t = \frac{V/S}{V_0} \tag{5}$$

where V_0 is the speed at which the droplet freezes. When V_0 was increased, the delay time of droplet icing decreased. When the droplet volume was constant, the larger the contact area was, the smaller the value of V/S, and the smaller the delay time of icing. Compared with the hydrophobic/superhydrophobic surfaces, the smooth surface had no micro/nanoscale pits. The contact area of the droplet with the smooth surface was the largest among the three surfaces, so the delay time of icing was the shortest. More air was trapped by the hydrophobic surface and superhydrophobic surface with a micro/nanocomposite structure than the smooth surface, which reduced the actual contact area of droplets with the solid surface and delayed the icing process.

In summary, the hydrophobic surface and the superhydrophobic surface had better anti-icing effects than the smooth surface. Compared with the smooth surface, the hydrophobic surface and superhydrophobic surface trapped air in their convex pit-shaped microstructures. Since air is a poor conductor of heat, heat transfer between the solid and liquid was reduced, and the icing process was delayed. With the same droplet volume, a large contact angle would increase the distance from the centre of gravity of the droplet to the solid surface, which would increase the thermodynamic barrier to ice core formation.

4. Stability test

4.1. Icing-melting test: To test the stability of the superhydrophobic aluminium alloy surface in practical applications, an icing-melting experiment was carried out. The experimental results are shown in Fig. 9.

Fig. 9 shows that the performance of the prepared superhydrophobic aluminium alloy surface was relatively stable. After up to 20 icing-melting tests, the contact angle and icing time did not change much. The roughness of the sample surface was measured using a laser confocal microscope, and the measurement results are shown in Fig. 10. Fig. 10 shows that the surface roughness of the test piece was slightly reduced as the number of icing-melting tests increased. Observation of the microstructure of the test piece by SEM revealed that the surface of the microstructure was not significantly damaged (Fig. 11). The change in roughness may be the main factor affecting the contact angle and anti-icing performance

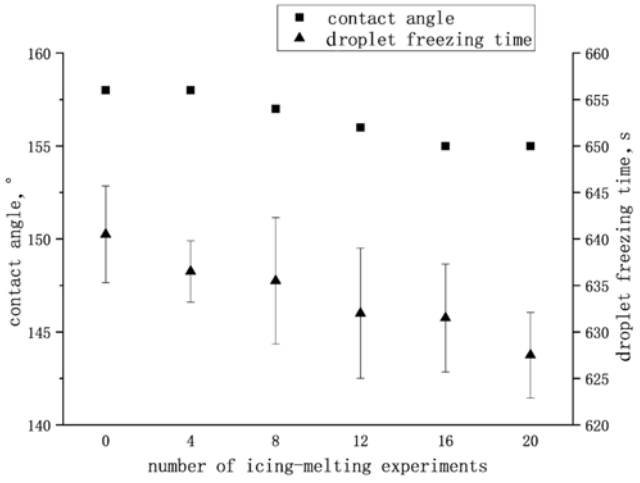

Fig. 9 *Contact angle and icing time after repeated icing-melting tests*

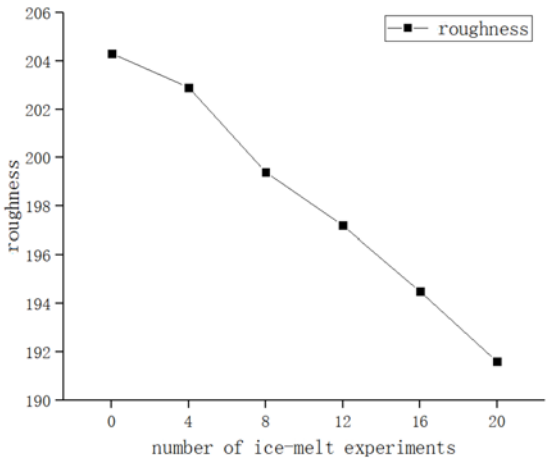

Fig. 10 *Roughness of the sample surface and the number of icing-melting experiments*

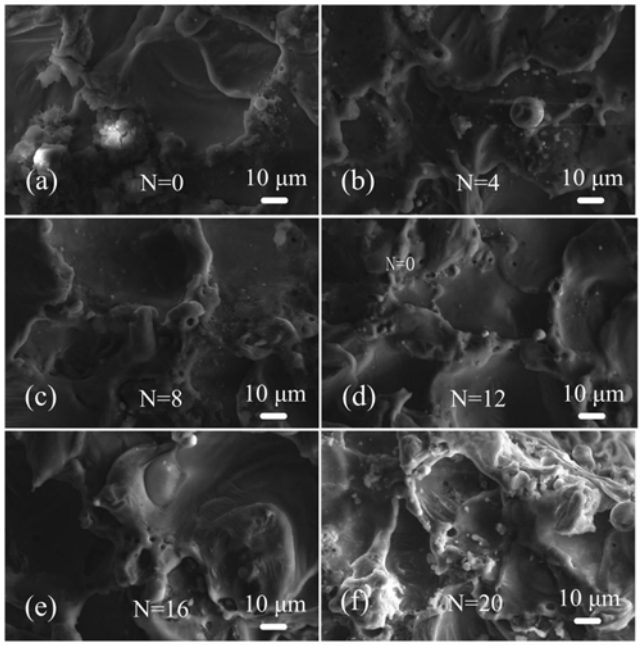

Fig. 11 *Microstructure following different numbers of icing-melting experiments (The number after N represents the times of ice-melting experiments)*

of the test piece [13]. The micro/nanoscale pits of the microstructured surface were slightly disrupted by the repeated icing-melting processes, which increased the actual contact area of the droplets with the surface and reduced the icing time.

4.2. Friction test: Because the damage to the surface microstructure caused by the freezing-melting test is small, a friction test was carried out to investigate the stability of the surface wettability and anti-icing performance of the samples.

Fig. 12 shows that when the number of friction tests was 10 and 20, the change in contact angle was within 5°, and the surface wettability was unchanged. However, when the number of friction tests was 30, the contact angle of the surface was drastically lowered by ~10°.

The wettability of the surface of the material was directly affected by the microscale convex pit-shaped structures on the surface of the square-column structure, so the wettability of the surface after friction testing was directly related to the integrity of the microstructure. Fig. 10 shows that in the case of slight friction (Figs. 13*a*

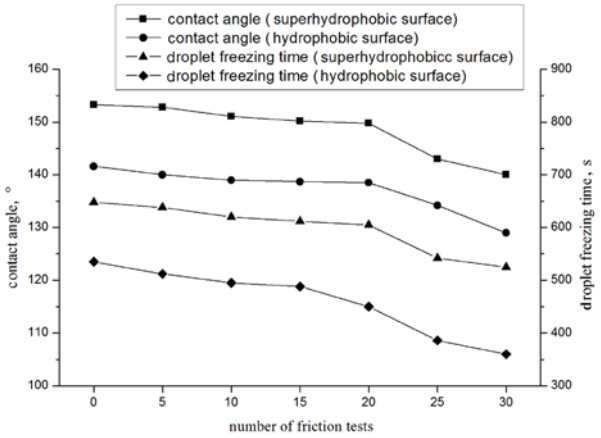

Fig. 12 *Friction test results*

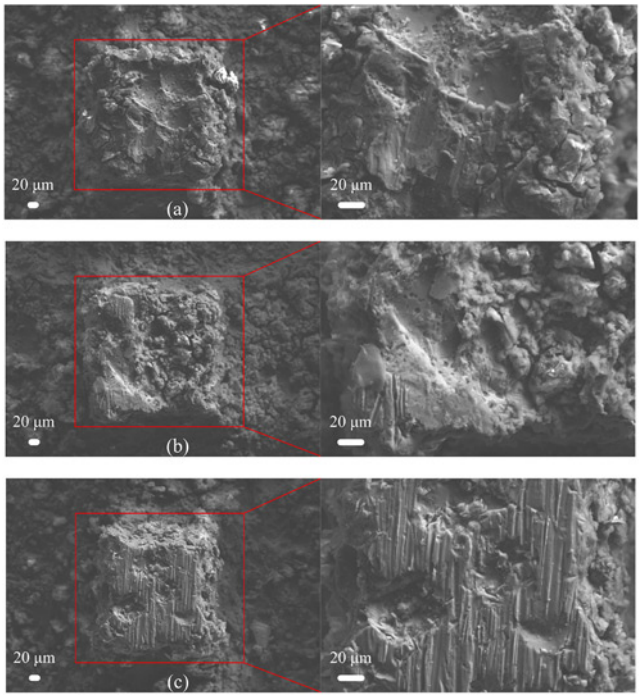

Fig. 13 *SEM images of the sample surface with different numbers of friction tests*
a 10 friction tests
b 20 friction tests
c 30 friction tests

and *b*), the micro/nanostructures on the square cylindrical surface were either not damaged or slightly damaged, and the pit and convex structures were relatively complete. Therefore, the hydrophobic properties of the surface were less affected. However, the micro/nanocomposite structures on the surfaces were destroyed by continuous friction (Fig. 13*c*), which reduced the hydrophobic properties of the aluminium alloy surface.

5. Conclusion: In the present work, aluminium alloy hydrophobic surfaces and superhydrophobic surfaces were obtained by using WEDM. Based on the characterisation of the hydrophobic/superhydrophobic aluminium alloy surface, the following conclusions were drawn:

(i) The square-column micro/nanocomposite structures on the surface of the aluminium alloy, which were fabricated by

doi: 10.1049/mnl.2019.0171

high-speed WEDM, produce an 'air cushion' effect and reduce the contact area between solid and liquid. One-step preparation of a hydrophobic/superhydrophobic aluminium alloy surface is achieved.

(ii) The wetting property of the material surface has a certain influence on its anti-icing performance. The hydrophobic/superhydrophobic surface produces the 'air cushion' effect because of its microscale convex pit-shaped structures and reduces heat transfer, thereby delaying the icing time.

(iii) The anti-icing effect of the hydrophobic/superhydrophobic surfaces decreases with decreasing temperature, but it is still superior to that of the smooth surface at the same temperature. Stability experiments show that the square-column composite structures on the surface have high environmental stability and mechanical strength.

6. Acknowledgments: This research was supported by the Jilin Province Science and Technology Development Program Funded projects of China (20180101324JC) and the Science and Technology Project of Jilin Provincial Education Department during the 13th Five-Year Plan Period (JJKH20190542KJ).

7 References

[1] Xu W., Song J., Sun J., *ET AL.*: 'Study on the characteristics of icing and frosting on the superhydrophobic surface of aluminum matrix', *J. Refrig.*, 2011, **32**, (4), pp. 9–13
[2] Yang Q., Luo Z., Tan S., *ET AL.*: 'Progress in anti-icing technology of superhydrophobic self-cleaning coatings', *China Surf. Eng.*, 2016, **29**, (4), pp. 10–22
[3] Fan Y., Liu X., Bai K., *ET AL.*: 'Research progress of anti-icing and melting coatings', *New Chem. Mater.*, 2014, **42**, (5), pp. 7–9
[4] Wang C., Chang S., Wu M., *ET AL.*: 'Numerical analysis of spattering characteristics of supercooled large water droplets', *Acta. Aeronaut. Sinica.*, 2014, **35**, (4), pp. 1004–1011
[5] Xiao C., Gui Y., Lin G.: 'Research progress and prospects of aircraft electric deicing', *Sci. Technol. Rev.*, 2011, **29**, (18), pp. 69–73
[6] Cheng S., Yu W., Wu W., *ET AL.*: 'Optimization of mechanical deicing sequence considering transmission line safety', *China Electr. Power*, 2018, **51**, (1), pp. 71–77
[7] Park E.J., Yoon H. S., Kim D. H., *ET AL.*: 'Preparation of self-cleaning surfaces with a dual functionality of superhydrophobicity and photocatalytic activity', *Appl. Surf. Sci.*, 2014, **319**, (1), pp. 367–371
[8] Yin X., Yu S., Hu J., *ET AL.*: 'Facile fabrication of a durable Ni_3S_2 nanorod arrays superhydrophobic surface with self-cleaning and degradation properties', *J. Alloys Compd.*, 2019, **791**, pp. 864–873
[9] Truesdell R., Mammoli A., Vorobieff P., *ET AL.*: 'Drag reduction on a patterned superhydrophobic surface', *Phys. Rev. Lett.*, 2006, **97**, (4), p. 044504
[10] Chen F., Lu Y., Liu X., *ET AL.*: 'Table salt as a template to prepare reusable porous PVDF-MWCNT foam for separation of immiscible oils/organic solvents and corrosive aqueous solutions', *Adv. Funct. Mater.*, 2017, **27**, (41), p. 1702926
[11] Mohamed A.M.A., Abdullah A.M., Younan N.A.: 'Corrosion behavior of superhydrophobic surfaces: a review', *Arab. J. Chem.*, 2015, **8**, (6), pp. 749–765
[12] Sarshar M. A., Swarctz C., Hunter S., *ET AL.*: 'Effects of contact angle hysteresis on ice adhesion and growth on superhydrophobic surfaces under dynamic flow conditions', *Colloid Polym. Sci.*, 2013, **291**, (2), pp. 427–435
[13] Li K., Zeng X., Li H., *ET AL.*: 'A study on the fabrication of superhydrophobic iron surfaces by chemical etching and galvanic replacement methods and their anti-icing properties', *Appl. Surf. Sci.*, 2015, **346**, pp. 458–463
[14] Thanh-Binh N., Seungchul P., Hyuneui L.: 'Effects of morphology parameters on anti-icing performance in superhydrophobic surfaces', *Appl. Surf. Sci.*, 2018, **435**, pp. 585–591
[15] Wang Y., Xue J., Wang Q., *ET AL.*: 'Verification of icephobic/anti-icing properties of a superhydrophobic surface', *Appl. Mater. Interfaces*, 2013, **5**, (8), pp. 3370–3381
[16] Farhadi S., Farzaneh M., Kulinich S.A.: 'Anti-icing performance of superhydrophobic surfaces', *Appl. Surf. Sci.*, 2011, **257**, (14), pp. 6264–6269
[17] Jin H., Li Z., Wei S., *ET AL.*: 'Corrosion resistance and dynamic anti-icing of superhydrophobic surface on ASW', *Surf. Eng.*, 2017, **34**, (5), pp. 1–8
[18] Barthlott W., Neinhuis C.: 'Purity of the sacred lotus, or escape from contamination in biological surfaces', *Planta*, 1997, **202**, (1), pp. 1–8
[19] Guo P., Zheng Y., Wen M., *ET AL.*: 'Icephobic/anti-icing properties of micro/nanostructured surfaces', *Adv. Mater.*, 2012, **24**, (19), pp. 2642–2648
[20] Liu Y., Li X., Yan Y., *ET AL.*: 'Anti-icing performance of superhydrophobic aluminum alloy surface and its rebounding mechanism of droplet under super-cold conditions', *Surf. Coat. Technol.*, 2017, **331**, pp. 7–14
[21] Huang Q., Xiong L., Deng X., *ET AL.*: 'Super-hydrophobic film deposition by an atmospheric-pressure plasma process and its anti-icing characteristics', *Plasma Sci. Technol.*, 2019, **21**, p. 5
[22] Cheng Y., Lu S., Xu W., *ET AL.*: 'Controllable fabrication of superhydrophobic alloys surface on copper substrate for self-cleaning, anti-icing, anti-corrosion and anti-wear performance', *Surf. Coat. Technol.*, 2018, **333**, pp. 61–70
[23] Jin H., Nie S., Li Z., *ET AL.*: 'Investigation on preparation and anti-icing performance of super-hydrophobic surface on aluminum conductor', *Chinese J. Chem. Phys.*, 2018, **31**, (2), pp. 216–222
[24] Laturkar S.V., Mahanwar P.A.: 'Superhydrophobic coatings using nanomaterials for anti-frost applications-review', *Nanosyst.: Phys., Chem., Math.*, 2016, **7**, (4), pp. 650–656
[25] Cassie A.B.D., Baxter S.: 'Wettability of porous surfaces', *Trans. Faraday Soc.*, 1944, **40**, (1), pp. 546–551
[26] Lian Z., Xu J., Wang Z., *ET AL.*: 'Fabrication and applications of two- and three-dimensional curved surfaces with robust underwater superoleophobic properties', *J. Mater. Sci.*, 2017, **52**, (2), pp. 1123–1136
[27] Zhang Y., Wu J., Yu X., *ET AL.*: 'Mass transfer characteristics of superhydrophobic copper surface on controllable array micro/nanostructures', *Acta Phys.-Chim. Sin.*, 2014, **30**, (10), pp. 001970–001978
[28] Piotr T., Marie L.M., David Q.: 'Delayed freezing on water repellent materials', *Langmuir the Acs J. Surfaces Colloids.*, 2009, **25**, (13), p. 7214